JURNAL TEKNOLOGI, Edisi No. 3. Tahun XIX, September 2005, 250-259 ISSN 0215-1685

Quantum-correlated Twin Photons from Sr_2O_2 Microstructure for 2.1 x 10^5 currie/mm Fast Thermal Neutron Floating

Moh. Hardiyanto
Institut Teknologi Indonesia – Serpong, Tangerang 15320
E-mail : moh_hardiyanto_iti@yahoo.com

Abstrak

Penelitian kami memperlihatkan suatu sumber dari pasangan foton dalam formulasi Abrikosov-Balseiro-Russell (ABR) menunjukkan adanya hamburan spontan pada mikro struktur Sr_2O_2. Berbagai korelasi kuantum memperlihatkan antara pasangan foton telah ditimbulkan melalui hamburan empat foton sekaligus dimana lompatan foton-foton tersebut ditimbulkan pada panjang gelombang 749 nm dengan aliran neutron termal cepat sebesar 2,1 x 10^5 currie/mm, dan sinyal serta foton-foton diam yang tidak digerakkan berlangsung pada panjang gelombang 737 nm dan 761 nm. Dalam sistem non-Abellian pada formulasi ABR, pendekatan kuantum akan menunjukkan keberadaan efek Cerenkov, sehingga reaktor nuklir Canadian Deuterium Uranium (CANDU) memakai matriks Sr_2O_2 untuk menghadang aliran 2,1 x 10^5 currie/mm neutron termal cepat sebelum timbul partikel anti-neutrino. Penelaahan yang cermat dari lompatan panjang gelombang dan polarisasi dalam kondisi Dirac menunjukkan pengamatan yang kritis pada korelasi-korelasi kuantum.

Kata kunci: *Pasangan-pasangan foton,Formulasi ABR, Mikro struktur Sr_2O_2, dan Lompatan panjang gelombang*

Abstract

Our research present a source of correlated photon pairs in Abrikosov-Balseiro-Russell (ABR) formalism that relies on spontaneous scattering in Sr_2O_2 microstructure. Quantum correlations are shown between photon pairs that are generated through four-photon scattering where the pump photons are degenerate at a wavelength of 749 nm with 2.1 x 10^5 currie/mm fast thermal neutron floating, and the signal also idler photons are nondegenerated at wavelength of 737 nm and 761 nm, respectively. In non-Abellian system for ABR formalism, the quantum approaching will be shown Cerenkov's effect existing, then the Canadian Deuterium Uranium (CANDU) nuclear reactor using by Sr_2O_2 matrix to be barier for 2.1 x 10^5 currie/mm fast thermal neutron floating before the anti- neutrino particle shown up. Careful adjustment of the pump wavelength and polarization in Dirac's condition are shown to be critical to observing quantum correlations.

Keywords : *Photon pairs, ABR formalism, Sr_2O_2 microstructure and The pump wavelength*

1. Introduction

Quantum entanglement between physically separated systems is a resource that is essential for implementing many quantum information processing. The vast majority of entangled-photon sources that are in use in various laboratories around the world today rely on spontaneous parametric down conversion in χ crystals. However, our research recently demonstrated a new type of source with Abrikosov-Balseiro-Russell (ABR) formalism in non-Abellian system [1] such as

$$\left| i \cong \sum_{\alpha} x_{\alpha}^{i} \left| \alpha \right> \right., \qquad (1)$$

which photon pairs were generated through non degenerate four-photon scattering. In ABR formalism, the parametric χ has resulted by a few equations consists of

$$\sum_{j}^{occ} \sum_{\beta\gamma\delta} \chi_{\beta}^{i*} \chi_{\gamma}^{j} \left(\mu\beta \left| V \right| \gamma\delta \right)$$

$$<\chi|CV|\gamma \equiv \sum_{\beta\delta} (\mu\chi\beta|V|\gamma\delta)\rho_{\delta\beta} \quad (2)$$

$$<\Phi|H\chi|\Phi^{\uparrow}> = \chi^{\bullet\bullet} \quad (3)$$

$$<\Phi|H\chi^{\bullet}|\Phi^{\uparrow}\chi^{\bullet}>> = \chi^{\downarrow} \quad (4)$$

$$\rho_{\delta\beta} = \sum_{j}^{occ} \chi_{\delta}^{j} \Phi_{\beta}^{j\bullet} \quad (5)$$

For fast neutron floating at 1.7 x 10^4 currie/mm, microstructure in Dirac's condition was symbolized by Φ and if not at Abellian-system was denoted by $\Phi^{\uparrow}$. This condition including of Schwinger transmutation by $\chi^{\bullet}$ and the invariant denoted by $\chi^{\downarrow}$ for non-Abellian system.

In this research, we present on measurement of correlations in the photon-pairs generated through four-photon scattering (FPS). The photon-counting experiments described herein provide a convincing demonstration of these correlations. The design of the experiment with Catch-Nuc and Interstellar Nuclear Beam equipments (Duprix, Hèlena, Dec. 2004) to produce correlated photon-pairs in dispersion-shifted Sr_2O_2 microstructure near 1550 nm wavelength [2].

The two fundamental differences between the work reported here and the earlier experiments are the wavelength of operation in 749 nm versus 1537 nm, and the use of a linear configuration as opposed to a Sagnac-loop configuration. After floating of 2.1 x 10^5 currie/mm fast thermal neutron in nuclear chamber, the barrier from Sr_2O_2 has resulted to be hold of anti-neutrino particle existing. This is a good condition before we continued to Dirac's condition after the neutron floating, and based on a few equations in ABR formalism, the quantum-correlations approaching will be adjustment the critical value of pump wavelength by Sr_2O_2 microstructure.

2. Theoretical Background

The classical theory of four-wave interactions in Sr_2O_2 microstructure has developed by ABR formalism with very simplicity equations such as [3]:

$$\frac{\partial A_1}{\partial z} = -\frac{\alpha}{2} A_1 + i\chi\left(|A_1|^2 A_1\right) \quad (6)$$

$$\frac{\partial A_2}{\partial z} = -\frac{\alpha}{2} A_2 + i\chi\left[2|A_1|^2 A_2 + A_3^{i\Delta kz}\right] \quad (7)$$

$$\frac{\partial A_3}{\partial z} = -\frac{\alpha}{2} A_3 + i\chi\left[2|A_1|^3 A_3 + A_2^{i\Delta kz}\right] \quad (8)$$

In these equations, $A_{1,2,3}$ are the field amplitudes of the pump, signal and idler waves, respectively, and α is the attenuation coefficient of the Sr_2O_2 microstructure according to $P(z) = P(0)e^{-\alpha z}$ where P is power and z is propagation distance. The nonlinier coefficient, χ, is related to the nonlinear refractive index, n_2, by $\chi = \frac{n_2\,\omega_1}{A_{eff}\,c}$, where A_{eff} is the effective mode area of the field, and ω_1 is the angular frequency of the pump. The wave vector mismatch is given by

$$\Delta k = 2k_1 - k_2 - k_3 \quad (9)$$

where k_1, k_2, k_3 are the wave vector magnitudes for the pump, signal, and idler waves. We have assumed that the pump is much stronger than the input signal and that group-velocity mismatch between the three waves is not significant; these are reasonable assumptions for the experiments described in this paper. The effects of linear loss, self-phase and cross-phase modulation are included, however.

For efficient interaction, solution of Eqs. (7-9) calls for the following phase-matching condition to be satisfied:

$$k = 2\chi P_1 + \Delta k \cong 2\chi P_1 + \beta(\omega_2 - \omega_1)^2 = 0 \quad (10)$$

where β is the group-velocity dispersion (GVD) coefficient and ω_2 is the angular frequency of the signal wave. The GVD parameter, D, is often used instead of β and they are related by $D = -\frac{2\pi c}{\lambda^2 \beta}$. In

ABR formalism after fast thermal neutron floating, but before anti-neutrino particle shown up, the simplicity equations change to quantum approaching with photon-pairs, explained like these equations:

$$<\Phi\left|\mathrm{H}\chi^{*}\right|\Phi^{\uparrow}>=\sum_{i}^{occ}<i\left|T\right|i_{k}^{\uparrow}>+\sum_{i<1}^{occ}\left(ij\left|V\chi^{*}\right|ij\right) \quad (11)$$

$$<\Phi\left|\mathrm{H}\chi^{*}\right|\Phi>=\sum_{i=1}^{occ}\sum_{\alpha,\beta}x_{\alpha}^{i^{*}}\chi_{\beta}^{i}<\alpha\left|\mathrm{T}\right|\beta>+$$

$$\frac{1}{2}\sum_{i,j}^{occ}\sum_{\alpha\beta\gamma\delta}x_{\alpha}^{i^{*}}\chi_{\beta}^{j^{*}}x_{\gamma}^{i}\chi_{\delta}^{j}\left(\alpha\beta\left|V\right|\gamma\delta\right) \quad (12)$$

$$\in_{k}\chi_{\mu}^{k}=\sum_{\gamma}x_{\gamma}^{k}\begin{pmatrix}<\mu\left|\mathrm{T}\right|\chi>\\+<\mu\left|v\right|\gamma>\end{pmatrix} \quad (13)$$

$$\rho=\sum_{j}^{occ}\left|j^{\downarrow}><j^{\uparrow}\right|$$

$$<r\left|\rho\right|r'>=\sum_{j}^{occ}<r\left|j^{\downarrow}><j^{\uparrow}\right|r'> \quad (14)$$

$$<r\left|\rho\right|r>\equiv\rho(r)=\sum_{j}^{occ}\left|\phi_{j}(r)\right|^{2} \quad (15)$$

In subsequent sections the FPS probability is approximated by calculating the classical power gain, G, for a weak pulsed signal whose spectral width is matched to that of the pass band of the detectors. The scattering probability, which is the same as the photon-pair production rate per pump pulse, is taken to be proportional to $G-G_0$, where G_0 is the "gain" when no pump is present. In the case of $\alpha=0, G_0=1$, but for loss Sr_2O_2 microstructure $G_0<1$ in ABR formalism without Abellian system.

The first formulation investigated by Arthuro J. Gomiez (Gomiez, J. Arthur, 2004) shown that the crystalline structure will be derived from BCS theory such as

$$H_{\mathrm{I}}=\sum_{i}J\left\lfloor C_{ki\uparrow}^{F}C_{ki\downarrow}^{F}\right\rfloor \quad (16)$$

The early equation was given by Abrikosov, Balseiro and Russel in matched on superconductivity crystalline structure (Duprix, Helèna, 2004) using Fermi's state non reactive electron cloud and Fermi-Hall reactive electron cloud. The completed equation was given by

$$H_{II}=\sum_{i}J\left\lfloor C_{ki\uparrow}^{F}C_{ki\downarrow}^{F}\right\rfloor+k\sum_{i}\sum_{j}\left\lfloor C_{kij\uparrow}^{F}C_{kij\downarrow}^{F}\right\rfloor \quad (17)$$

3. Microstructure Sr_2O_2 properties

The analysis described above applies equally well to four-photon interactions in any type of Sr_2O_2 nuclear structure. The advantages of using quantum correlations for demonstrating nonlinear-Sr_2O_2 nuclear structure effects arise from several novel properties: the nonlinear coefficient is enhanced in small-core a few μm^2 which support a single transverse mode over an extremely broad wavelength range (370 nm – 1600 nm). These four properties combine to allow efficient interactions to occur FPS which are either much less efficient or not possible at all in standard Sr_2O_2 nuclear structure.

Table 1.
Various properties of the Sr_2O_2 nuclear structure in FPS

Sr_2O_2 properties	Value
Length	0.98 m
Core diameter	1.7 μm
Attenuation	86 dB/m
Cutoff wavelength	< 530 nm
λ_0	Mode A : 749 ± 3 nm Mode B : 743 ± 3 nm
D_{slope}	Mode A : 0.64 ps Mode B : 0.68 ps
γ	97.5 (W m)$^{-1}$

Source : courtesy of CANDU nuclear reactor based on our research no. 019/2004, Canada

The zero-dispersion wavelength, λ_0, and the slope of GVD curve, D_{slope}, near λ_0 are determined experimentally by measuring the wavelength dependent group delay in an interferometric configuration. The group delay is then plotted as a function of wavelength and fitted to a low-order polynomial up to χ^2 or χ^3. The first derivative of the group-delay curve, normalized to the length of the Sr_2O_2 microstructure under test, the gives the parameter GVD, *D*. The Dirac's condition will be supporting to existing of twin-photons at Abellian-system. Using by quantum approach, the resonances of twin-photons will be detected by trans-Thorium derivation (Duprix, Helèna, 2004) when the fast neutron was breaking on Dirac's condition at Josephson's tunelling. The other side, with Born's approximation will give the interstellar *duplet* functions at Sr_2O_2 microstructure [4].

These experiments using by a few nuclear beam equipments such as Volkov's dectector and Control room of nuclear chain reaction, are shown in Fig. 1 and 2.

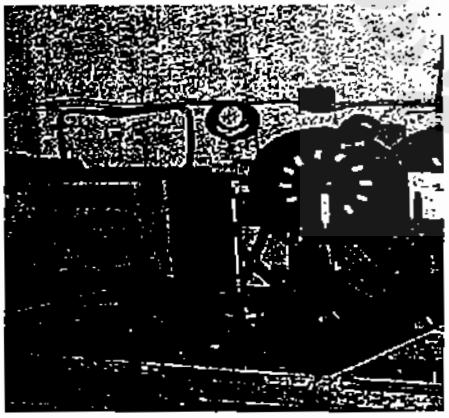

Figure1.
Volkov's Detector for measurement of photons and thermal neutron existing after Cerenkov's effect for 400-510 tesla magnetic field at 45.7 MW adjusted power nuclear reactor.
(Courtesy and special permission of CANDU Nuclear Reactor, 2004, Canada)

A few experiments using by Volkov's Detector and control room for detecting of neutrino particles after Cerenkov's effect has been resulted to match for analytical approaching, especially for 1.7 until 2.1 x 10^5 currie/mm neutron floating. Based on the derivation of ABR formalism to Sr_2O_2 microstructure, a few hypothesis equations will be tested by several experiments, particularly for tunelling effect after bounding reaction, at Thorium decay.

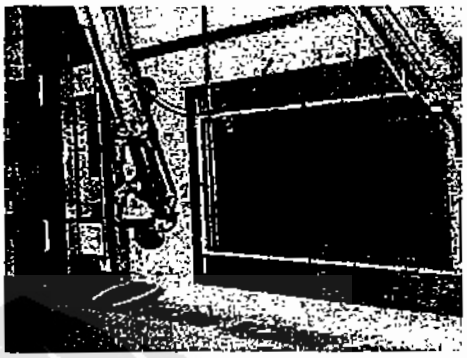

Figure 2.
Control room of nuclear chain reaction for measurement of neutrino particles and thermal neutron existing after Cerenkov's effect for 450-620 tesla magnetic field at 45.7 MW adjusted power nuclear reactor. (Courtesy and special permission of CANDU Nuclear Reactor, 2004, Canada)

Results for group delay measurements taken for the FPS used in these experiments are shown in Fig. 3.

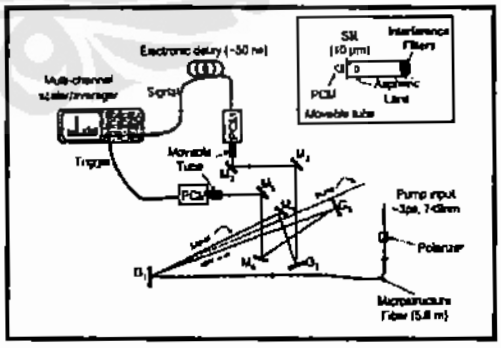

Figure 3.
A schematic of the experiment used to generate and detect quantum correlated twin photons generated in FPS.
(Courtesy of CANDU Nuclear Reactor, 2004, Canada)

In fig. 3. the two curves correspond to the two polarization modes of the MF, revealing that the group delay behavior is

quite different between the two polarization modes. The lines given with the data are fits to the second-order polynomial function,

$$\text{Delay} = a\lambda^2 + b\lambda + c, \qquad (18)$$

where for Sr_2O_2 material $\lambda_0 = 749$ nm: $a = 0.321, b = -481,$ and $c = 180000$; and for Sr_2O_2 microstructure $\lambda_0 = 743$ nm: $a = 0.338, b = -502,$ and $c = 186000$. In the inset of Fig. 1 are plots of the first derivative of the fitted curves, revealing the fact that λ_0 is not the same for the two polarization modes. Other important parameters of the MF used herein pertaining to FPS especially for Sr_2O_2 material are summarized in Table 1.

For these experiments based on quantum approximation at ABR condition, such as

$$H_{II} = \sum \varepsilon_k C_{ka}^F - \hbar\Delta \sum \left\{ C_{k\uparrow}^F \, C_{k\downarrow}^F x \hbar c \right\} \qquad (19)$$

$$\Delta = g_{BCS} \sum_k \left\langle C_{k\downarrow} \bullet C_{k\uparrow} \right\rangle \qquad (20)$$

Concerning of crystalline microstructure for $Sr_2\ O_2$ material for it's crystalline structure reliable value, there is a few points for analyzing that phenomena such as:

a. The Compton's displacement wave length has very smooth waving on top side, it means for 0.811752 / 10^{-3} amu magneton's nucleus, the phonon-electron cloud together with Fermi-Dirac state and neither of one pieces of thermal neutron could be breaking the barrier on 10^3 nm depth area.
b. At adjusted power 45.7 MW and 2.1 x 10^4 currie/mm luminosity of fast thermal neutron floating, the interstellar of this material able to conduct of quantum semi-relativistic electrical charge, the amount is 7.8114/eV. It can be calculated by Equations (14) and (16) in group-theory, but with quantum coupling rotation for magnetic-rotate has shown by

$$P^2 = J(J+1)\hbar^2; \quad \text{requirement : } \mathbf{J} = 0,1,2,\ldots \qquad (21)$$

$$P_z^2 = M^2\hbar^2 \quad ; \text{requirement: } \mathbf{M} = 0, \pm1, \pm2, \ldots \mathbf{J} \qquad (22)$$

$$P_k^2 = K^2\hbar^2 \quad ; \text{requirement: } \mathbf{K} = 0, \pm1, \pm2, \ldots \mathbf{J} \qquad (23)$$

4. Four-photon scattering experiments

The experimental setup that was used to study photon-pair production in MF is shown in Fig. 3. Linearly polarized, ~3 *ps*-long pump are launched into a 5.8 m-long MF such that the plane of polarization is aligned along one of the polarization-mode axes of the fiber. The choices of pump wavelength and which MF birefringent axis is used are critical as will be discussed in more detail later. For low pump powers, as the pump pulses propagate through the fiber, there is a small probability that a four-photon parametric scattering event will occur. The resulting signal and idler photon pairs co-propagate along with the pump and emerge from the MF.

According of quantum magnetic-spin and magnetic-resonance which are expressed by Equations (11) until (22) that was describing about how strongest impact from thermal neutron bombarding to Fermi-Dirac interstellar area wide. However, the wide is 0.001127 x 10^{-10} meters having magnetic field deflection on resonance of spin-rotate around 6772.55 cm per each Fermi's cloud active reaction. This matter in 500 MHz up to 550 MHz magnetic-spin frequency with Na_2SO_3 liquid moderator's water cooling at reactor chamber. For show up the impact and existing of Fermi-Dirac's surface effect caused by Anderson's tunnel for floating of thermal neutron electrical charge in quantum magnetic-spin also resonance, it has figure out from Gell-Mann spectroscopy.

As a consequence of choosing the linear configuration, spectral filtering is quite difficult. Photon pairs emerge from the MF accompanied by a very strong pump field. Given a pump pulse containing $\cong 10^7$

photons, numerically solving Eqs. (1-3) in the presence of loss predicts that the FPS probability is about 17%. Therefore, the output of the MF consists of a large number of pump photons and an extremely small number of spontaneously scattered signal and idler photons that are separated in wavelength from the pump by ~10 nm. For efficiont detection of the signal-idler pairs, pump-photon suppression by greater than 90 dB is required. We obtain this suppression by use of three diffraction gratings (Richardson Grating Laboratories, 600 lines/mm, nominally blazed for 800 nm) arranged so that two different spectral regions can be detected on separate photon-counting modules (PCMs). The PCMs are commercially available devices (Perkin-Elmer, model SPCM-AQR-16), which count individual photons at 750 nm wavelength with a quantum efficiency of ≅ 75%. Each time a photon is detected by the PCM it generates a 5 V pulse of 30 ns duration. Counts are registered using either a gated photon counter (Stanford Research Systems, model SR-400) or a multi-channel scaler/averager at Osaka University, Japan.

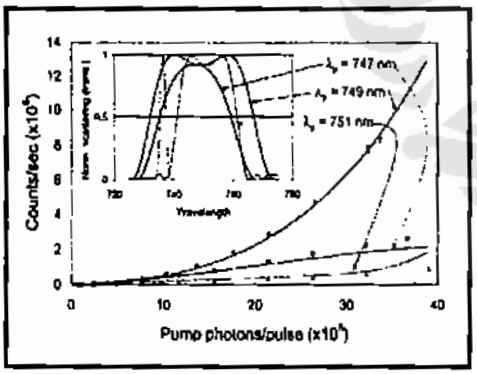

Figure 4.
Graphs showing the spectral response of the detection filter in comparison with the bandwidth of the injected pump. Note that the passband centers of the detection filter for the signal and idler are located symmetrically with respect to the pump's center wavelength, and that the detection bandwidth (2.1 nm FWHM) is considerably larger than the pump bandwidth (0.3 nm FWHM). (Courtesy of CANDU Nuclear Reactor, 2004, Canada)

The dark-count levels for the two detectors are typically ~25 counts/s for the signal detector and ~140 counts/s for the idler detector.

The output from the MF is directed onto the first diffraction grating, G_1. A mirror (M_1 in Fig. 4) is used to direct the long wavelength (signal) portion of the spectrum to a second grating, G_2. while the short wavelength (idler) portion passes the mirror and hits a third grating, G_3. As such, the signal and idler are diffracted twice each. The diffracted waves are then directed through interference filters whose purpose is twofold: to provide additional filtering of the pump and to block the ambient room light. The Ifs are specified to have 10 nm pass bands centered at either 740 nm or 760 nm. The pass band center of these its can be tuned in wavelength by slightly rotating them such that the incident wave is no longer normal to the surface.

Table 2.
The properties of quantum magnetic field states

Materials	Quantum magnetic-spin value	Quantum states
Sr_2O_2	7.1006/eV	$C^F_{kij\uparrow}; E_{(FD,J)}$
	7.8114/eV	$C^F_{kij\uparrow}; E_{(FD,P,J)}$
	7.7221/eV	$C^F_{kij\uparrow}; E_{(FD,J)}$

Source : courtesy of CANDU nuclear reactor based on our research no. 019/2004, Canada

Finally, the signal and idler each pass through an aspheric lens ($f = 11$ nm) and a 10 μm slit to achieve the desired specral filtering. The detection filter optics are arranged so that the strong pump wave passes without being scattered by any surface until it is dumped onto a black surface. In addition, the number of optical elements that are used in the filter system is minimized in order to reduce unnecessary scattering of light from surfaces and imperfections.

The transfer characteristic of the detection filter is shown in Fig. 4. Here the relative count rate (in dB) on each photon counter is shown as a function of the wavelength for an injected signal. The

spectrum of the input pump pulse is included to show that the center wavelength of the pump is placed symmetrically in between the pass bands of the detection filter. The 3 dB bandwidth of each of the two pass bands is 2.1 nm, which is large compared with the spectral width of the pump (~0.3 nm). The peak total detection efficiency at the center of each pass band of the filter (including the quantum efficiency of the respective PCM as well as propagation losses from the fiber to the PCM) is about 4 ± 1%.

Even if, prior to detection, one is able to perfectly filter away photons at the pump wavelength, one also has to take great care to ensure that there are no photons injected into the MF whose wavelengths correspond to that of the signal and/or the idler. Use of a pulsed pump implies that are photons in the spectral sidebands of the pump at the input to the MF. These extra photons could cause stimulated FPS rather than the spontaneous FPS we are seeking. Therefore, to achieve suppression of the pump sidebands, we pass the pump wave through a double grating monochromatic before injecting it into the MF. This yields a pump sideband suppression in excess of 100 dB. The double grating monochromatic also filter the pump pulses, yielding a narrow pump bandwidth of ~0.3 nm.

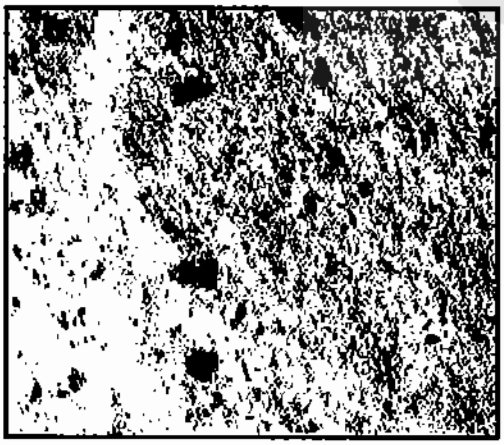

Figure 5.
The Sr_2O_2 material after Josephson's tunneling with two photons-pair a given detection filter setting for $\lambda_0 \sim 740$ nm. (Courtesy of CANDU Nuclear Reactor, 2004, Canada)

Data points are accompanied by theoretical scattering curves, which were fitted to the data using Eqs. (1-3). The λ_0 is assumed to be 748 nm for these calculations. One sees that the optimum response is achieved for a pump wavelength of 749 nm. The dashed curve in the inset shows the measured filter response for the idler passband in comparison with the theoretical of FPS efficiency versus wavelength. Width is desirable because the system then more closely approximates what is expected for a CW pump.

Proper choices of the pump, signal, and idler wavelengths, and careful alignment of the system are critical to obtaining the desired result. As can be seen in Fig. 5, the choice of pump wavelength and the detection filter pass band wavelengths with respect to the fiber's λ_0 have a dramatic effect on the FPS phase-matching bandwidth and, consequently, the signal-idler pair production rate. The filter and pump wavelengths must be chosen so that the pass bands of the detection filter are near the peaks of the phase matching curve, as is the case for $\lambda_p = 749$ nm.

We made FPS measurements for the idler photon counts as a function of the pump power, and the results are shown in Fig. 5. The fiber's polarization mode corresponding to $\lambda_0 \cong 749$ nm was excited with pump pulses whose wavelength varied from 747 nm to 751 nm. It is evident that the count rate is dramatically reduced for pump pulse of wavelengths detuned from λ_0 by more than ± 2 nm. In practice, detouring the pump wavelength by more than ± 1 nm from the optimum value reduces the pair production rate so dramatically that the background noise level due to leaked light and dark counts is dominant. Recall that the fiber's λ_0 is polarization dependent due to birefringence in the MF (see Fig. 3.). This means that the polarization of the pump also dramatically affects the signal/idler count rate in the experiment.

The viewing in Fig. 5 has been fitted to theory by numerically solving Eq. (1-3) to calculate the power gain, G, and then scaling the numerical results according to

$$R = a_1\left[(G - G_0) + b_1\left(P_{pump}\right)\right], \qquad (24)$$

where R is the *total detected photon scattering efficiency* per pump pulse, G_0 is the gain when the injected number of photons per pump pulse $\left(P_{pump}\right)$ is equal to zero. The fitting parameter $a_1 = 0.027$ counts/pulse is the total photon detection efficiency, which agrees within the margin of error with the independently measured value of 4 $\pm$ 1%. The fitting parameter $b_1 = 8.7x10^{-9}$ counts/photon is the leakage through the detection filter and/or the contribution of spontaneous Raman scattering. In this experiment, FPS, Raman scattering, and linear loss are all of the same order of magnitude. As a result, it is difficult to quantify the contribution due to Raman scattering without a more comprehensive theory, shown up for Sr_2O_2 material after Josephson's tunneling.

Joining between Coulomb nuclear force with Bohr's centripetal force in relativistic quantum area, which is 2.1 x 10^4 currie/mm thermal neutron flux absorption for minimal condition in reactor chamber, the value of *n*-th stage begin from 1 up 2 according the Fermi's interference condition. Based on the formulation for Fermi-Dirac's active cloud in coherent Compton's wave length, will be adjoined of critical modulation phonon's vibration and Cooper's pair cloud.

To detect temporally coincident counts using the multi channel scaler, the output from one of the PCMs is used as trigger input to the scaler while the pulses from the other PCM are measured at the signal input of the scaler. The instrument then generates a histogram of the arrival time of signal pulses with respect to the trigger pulses. A typical set of data recorded by the scatter is shown in Fig. 4, where it can be seen that one of the peaks is much taller than the others. The peak is evidence of a higher probability of registering a count on the signal PCM in the same time window as the count registered on the trigger PCM. The other peaks are spaced from each other by 13 ns (modulo 5 ns due to the bin resolution limitation on the scaler) and arise due to the fact that pulsed pump at 75-MHz repetition rate is used. One can clearly see the 13 ns repetition period on the histogram.

Figure 6.
Sr_2O_2 scattering material scaler where one counter is used to trigger the acquisition and the order is taken to be the PCMs signal at 450 tesla. (Courtesy of CANDU Nuclear Reactor, 2004, Canada)

Data from the scaler can be used to make a comparison between the rate of coincidences versus non-coincidences. A plot of coincident counts registered and non-coincidence counts registered as a function of the number of pump photons per pulse. This plot clearly demonstrates that more coincident photons are generates at the signal/idler wavelengths than the accidental coincidences that result from the background photons.

The coincidence counting results in Fig. 6 do show the existences of correlated photons, but only on top of a large background of accidental coincidence counts. The "true coincidence counts" are obtained by subtracting the accidental coincidence counts from the total coincidence counts (Harold, Thomas S, Dec. 2004). While we expect a quadratic variation, we observe that the true coincidence count rate varies slightly sub-linearly with pump power. The origin of

this discrepancy is unclear at this time. The accidental coincidences may arise from mechanisms such as pump leakage due to imperfect filtering, but it is highly that the bulk of these accidental counts arise from spontaneous Raman scattering. Recently, we have presented a quantum theory of the four-wave interactions in fibers with systematic inclusion of the Raman effect.

A quantitative comparison with this theory is underway and will be presented elsewhere. If one makes the comparison between the results presented here and those of Florence Matinne experiments, we expect the coincidence-to-background ratio to be much worse for the choise of wavelengths used here because the signal wavelengths falls much closer to the peak of the Raman gain curve.

The quality of the correlated photons generated by FPS in the MF id limited by the high rate of accidental coincidences. Accidental coincidence counts due to imperfect filtering as well as from spontaneous Raman scattering could be dramatically reduced if the signal and idler photons are generated with greater wavelength separation from the pump. In a recent paper, Helèna Duprix describe measurements of modulation instability in highly nonlinear MFs where the signal- and idler-to-pump detuning exceeds 100 nm. This wavelength separation would result in photon pairs being generated away from the peak of the Raman gain, which can then be efficiently filtered from each other as well as from the pump photons.

When starting the experiment, we had hoped to create polarization entanglement by pumping both polarization modes of the MF simultaneously. However, it is clear from the data presented in Fig. 4 that optimum pair production depends upon choosing a pump wavelength almost exactly equal to the λ_0 of the fiber. Since the two polarization modes of the fiber have λ_0 differing by about 5 nm, this approach will not work because the efficiency of the FPS process must be the same in both polarizations. However, it is still possible to generate polarization entanglement by using a counter-propagate pump configuration wherein one polarization mode of a MF is pumped in both directions at the same time. By including a 90-degree twist in the fiber orientation, and mixing the two output (orthogonally pillaged because of the twist) using a polarization beam splitter, polarization entanglement can be produced.

5. Conclusions

In conclusion, we have studied the coincident nature of photon-pairs created in MF due to FPS. We have shown that in order to detect photon correlations one must understand the group velocity dispersion and polarization properties of the fiber being used.

a. The strength of thermal neutron flux absorbed is 2.1 x 10^5 currie/mm for twin photons microstructure of Sr_2O_2.
b. At thermal neutron flux amount 2.1 x 10^5 currie/mm then the value of quantum magnetic-spin is 7.8114/eV and Josephson's tunnelling between interstellar area around 737 nm and 761 nm, then the thermal neutron electrical charge could be flowing smoothly.

Polarization dependent dispersion behavior in MF provides unique challenges for the generation of polarization entanglement.

This research was supported in part by the Canadian Deuterium Uranium (CANDU) nuclear reactor a collaborative Royal Canadian Education Affair grant (CNAD19-00-1-0177)

References

1. Beiser, Arthur, Earth Sciences, New Edition, Me-Graw Hill Book Company, New York, 2001, pp. 145-177.
2. Betingthon, Dominique F., "Making of Control Rod Blade in Magnetic Stirrer", CANDU Nuclear Reactor of Canada Atomic Journal, 18, 2003, pp. 111-125.

3. Canadian Deuterium Uranium (CANDU) Nuclear Reactor, Report of Material Testing at 450 tesla, Vol. 3, 2004, pp. 16-28.
4. Chalotra,G.P.,Electrical Engineering Materials, Khana Publishers, New Delhi, 2001, pp. 156-177.
5. Chattopadhyay, C., and Rakshit P.C., Quantum Mechanics and Solid State Physics, Mc-Graw Hill Book Co., New York, 2001, pp. 144-169.
6. Durant,W.C., "Manufacturing of Control Rod Blade by Simulation", Journal of PWR and BWR Reactor, 15, Dec. 2004, pp. 156-164.
7. Duprix, Helèna, "The Measurement of Sr_2 Matrix with Quantum Approximation", NASA Report, Vol. 12, December 2004.
8. Gomiez, Arthuro J., "Idle Time and Power in Sr_2O_3 . H_2O for High Energy", British Atomic Energy Journal, 69,Dec. 2004, pp.77-89.
9. Harold, Thomas S., "Unsteady Condition for Sr_2O in Multi Purpose Reactor", British Atomic Energy Journal, 69,Dec. 2004, pp. 101-114.
10. Kempster, M.H.A., Materials for Engineers, Mc-Graw Hill Book Co., New York, 2001, pp. 210-221.
11. Stuart, Thomas P., "Muon Particle to be Absorbed by Sr_2Cr_3O in PWR", IAEA Journal, 48, Jan. 2005, pp. 85-99.
12. Thorton, Ian, "Preorientation Sr_2O_2 Compound in Control Rod Blade", CANDU Reactor of Canada Atomic Journal, 18, Nov. 2003, pp. 77-89.
13. Valli, G., "The Experimental Programme for the Development of The Multi Purpose Reactor", IAEA Journal, 48, Jan. 2005, pp. 141-145.
14. Vasudeva, D.N., Fundamentals of Magnetism and Electricity, S. Chand and Company Ltd., New Delhi,2001, pp. 79-85.
15. Vialli, T., "ABR Formulation for Sr_2O_2 Moderator Material", IAEA Journal, 47, Dec. 2004, pp. 87-99.
16. Waghmare,Y.R.,"Strontium Elements in Multi Purpose Reactor at 45 MW, CANDU Reactor of Canada Atomic Journal, 18, 2003, pp. 61-70.
17. Weigner, Karl P., "Buffer Element of Thermal Neutron Flux in CANDU", CANDU Reactor of Canada Atomic Journal, 18, 2003, pp. 71-84.